ATTITUDE AND ORBITAL DYNAMICS MODELING FOR AN UNCONTROLLED SOLAR-SAIL EXPERIMENT IN LOW-EARTH ORBIT

Laura Pirovano[(1)], Patric Seefeldt[(2)], Bernd Dachwald[(3)], and Ron Noomen[(4)]

[(1)]*Faculty of Aerospace Engineering, TU Delft, Kluyverweg 1, 2629 HS Delft, The Netherlands, +31 645788373, l.pirovano@student.tudelft.nl*

[(2)]*Institute for Space Systems, German Aerospace Center (DLR), Robert-Hooke-Str. 7, 28359 Bremen, Germany, +49 421244201609, patric.seefeldt@dlr.de*

[(3)]*Faculty of Aerospace Engineering, FH Aachen University of Applied Sciences, Hohenstaufenallee 6, 52064 Aachen, +49241600952343, dachwald@fh-aachen.de*

[(4)]*Faculty of Aerospace Engineering, TU Delft, Kluyverweg 1 2629 HS Delft, The Netherlands, +31 152785377, r.noomen@tudelft.nl*

Abstract: *Gossamer-1 is the first project of the three-step Gossamer roadmap, the purpose of which is to develop, prove and demonstrate that solar-sail technology is a safe and reliable propulsion technique for long-lasting and high-energy missions. This paper firstly presents the structural analysis performed on the sail to understand its elastic behavior. The results are then used in attitude and orbital simulations. The model considers the main forces and torques that a satellite experiences in low-Earth orbit coupled with the sail deformation. Doing the simulations for varying initial conditions in attitude and rotation rate, the results show initial states to avoid and maximum rotation rates reached for correct and faulty deployment of the sail. Lastly comparisons with the classic flat sail model are carried out to test the hypothesis that the elastic behavior does play a role in the attitude and orbital behavior of the sail.*

Keywords: *Solar sail, Gossamer structures, Attitude dynamics, Orbital dynamics*

1. Introduction

Lightweight deployable spacecraft structures, often referred to as Gossamer structures, have attracted the attention of researchers in recent years. Examples for such developments are technology demonstration of solar sail technology or drag sails for a faster de-orbit of low-Earth orbit (LEO) satellites [1, 2, 3, 4, 5, 6, 7, 8, 9]. This recent focus has increased the need for attitude analysis of such elastic structures in order to allow engineers to incorporate the deployment and operational loads in the sizing process. In the last years, the German Aerospace Center (DLR) has developed technologies that allow an autonomous deployment of membrane spacecraft structures such as solar sails, drag sails and thin-film photovoltaics [10, 11]. The development was carried out in DLRs Gossamer-1 project. The aim of this project is a low-cost technology demonstrator. Within this project, scalable deployment technologies including membranes, booms, photovoltaics and their corresponding mechanisms are developed. The mission objective is the demonstration of a successful and reliable deployment in LEO. Figure 1(f) provides an artist's impression of the deployed Gossamer-1 sail. For a demonstration in the LEO environment, it is necessary to understand the attitude behavior of such a satellite which is dominated by aerodynamic drag, solar radiation pressure and gravity gradient torques. Within the ongoing European Space Agency (ESA) projects "Deployable Membrane" and "Architectural Design and Testing of a De-orbiting Subsystem" DLRs Gossamer-1 technology was the basis for the development of a pyramidal shaped

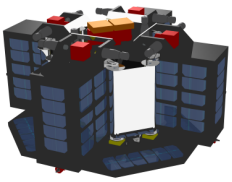

(a) Launch configuration, approx. 30 kg, height=500 mm, width=790 mm

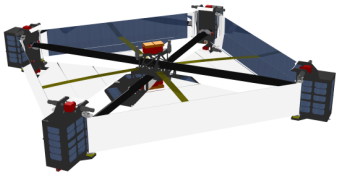

(b) Start of Deployment

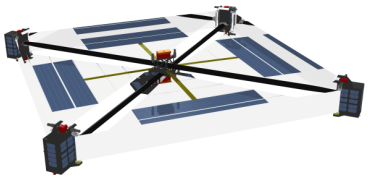

(c) During deployment

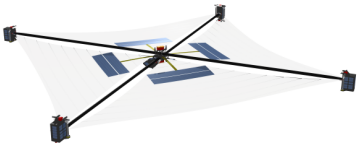

(d) Deployed

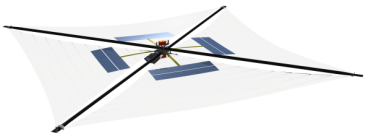

(e) Deployed and mechanisms jettisoned, approx. 10 kg, $5 \times 5\,\mathrm{m}^2$ sail area

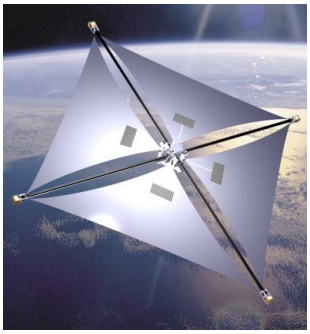

(f) Artist's impression of the sail in low-Earth orbit

Figure 1. Gossamer-1 deployment sequence.

drag sail. The development of the drag sail is carried out in a consortium consisting of the companies High Performance Space Structures GmbH, Hoch Technologie Systeme GmbH, Etamax Space GmbH and DLR. The aim of the development is a self-stabilizing drag sail. This development also highlights the need for an adequate attitude analysis methods for large elastic structures interacting mainly with drag and solar radiation pressure. The analysis presented in this paper is focusing on in-orbit simulation of the Gossamer-1 deployment technology demonstrator. The satellite would have a mass of about 30 kg and a sail size of $25\,\mathrm{m}^2$. In Fig. 1 the deployment sequence of the Gossamer-1 sail is shown. Starting from a very compact launch configuration, the sail is deployed with boom system deployment units (BSDUs) that are moving from the center of the satellite to the outside. At the end of the deployment an optional jettison of the mechanisms is possible. This jettison of the deployment units is one central part of the solar sail use case, to shed dead mass. This is in order to minimize sailcraft loading and thereby maximize the characteristic acceleration that can be reached with solar sailcraft. Of course jettison would take place on an Earth escape trajectory and not in LEO where it would cause additional space debris. Based on a structural analysis of the deployed sail, which is billowing under atmospheric drag, the geometry is simplified as described in Section 2. The main perturbations that influence the sail motion are drag, solar radiation pressure, the first zonal harmonic of the Earth gravitation field J_2 and the gravity gradient. The equations of motion integrate both the translational and rotational motion due to the coupling resulting from the perturbations included and a six-degree-of-freedom state vector is formulated in a thirteen-parameter vector, thus containing coordinates for position, velocity, attitude and angular

velocity of the satellite. The equations are implemented in Matlab and integrated using the `ode113` solver. The result is an impression of the orbital and rotational behavior of the satellite over time depending on the initial conditions.

2. Billowing prediction

For the analysis of the billowing of the sail a finite-element model was created in ANSYS Workbench 15. The sail geometry, including areas with thin film photovoltaics, was modeled with the CAD tool CATIA V5R20. From that model a simplified version for the analysis was derived. The model consists only of surfaces and the geometry as shown in Figure 2 was considered. The simplified model only shows one half of one sail segment. When further processed in the finite-element analysis the symmetry of the segment was used to reduce computational effort. The Catia CAD

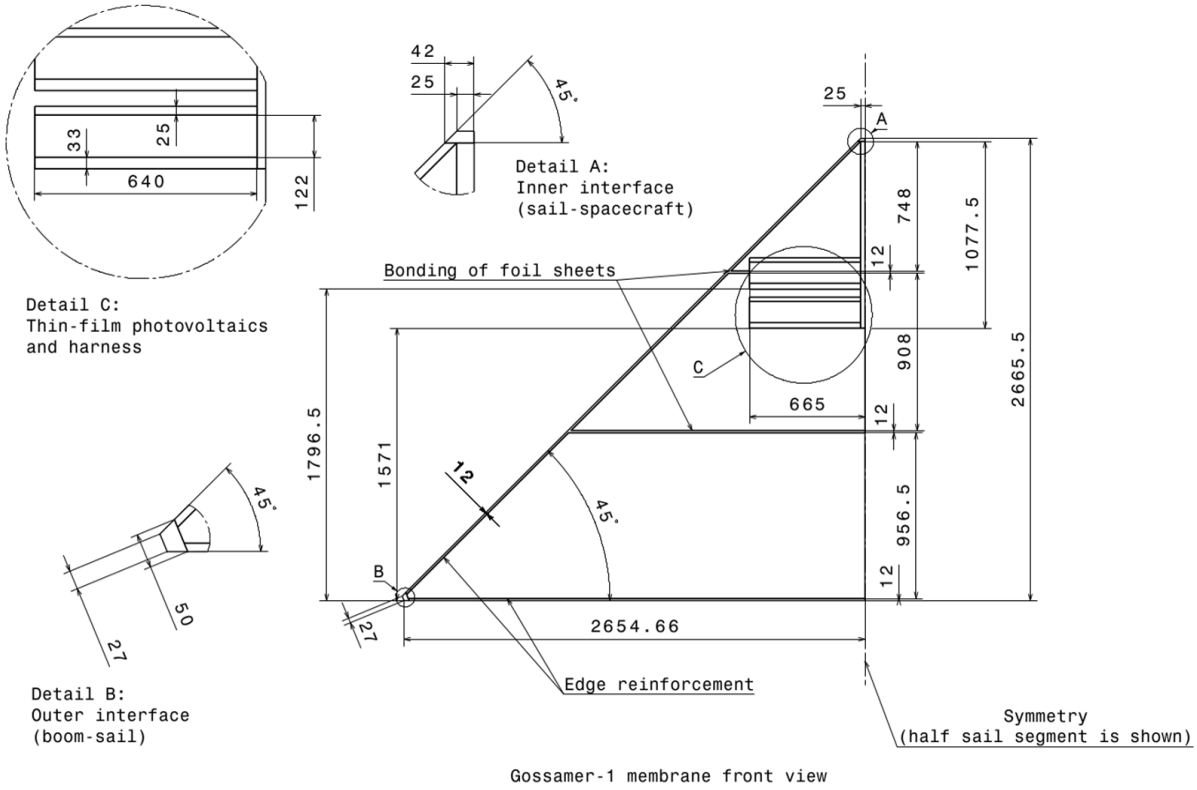

Figure 2. Drawing of the simplified Gossamer-1 membrane forwarded to finite-element simulations. Note that only the half sail segment is shown and that the sail is symmetric to the height of the triangular-shaped full sail segment.

model, which only consists of surfaces, was imported into ANSYS Workbench. In this way the software automatically applies shell elements to the areas. The sail is very thin, especially compared to its other dimensions. In consequence, it is common for those structures to use two-dimensional shell elements instead of modeling the complete body, which would also require very small elements to resolve the thickness properly and in consequence would dramatically increase the computational effort. Figure 3 gives an overview of the finite-element model. When tensioning such a thin membrane it will always result in a wrinkling surface. The wrinkling pattern appearing on a

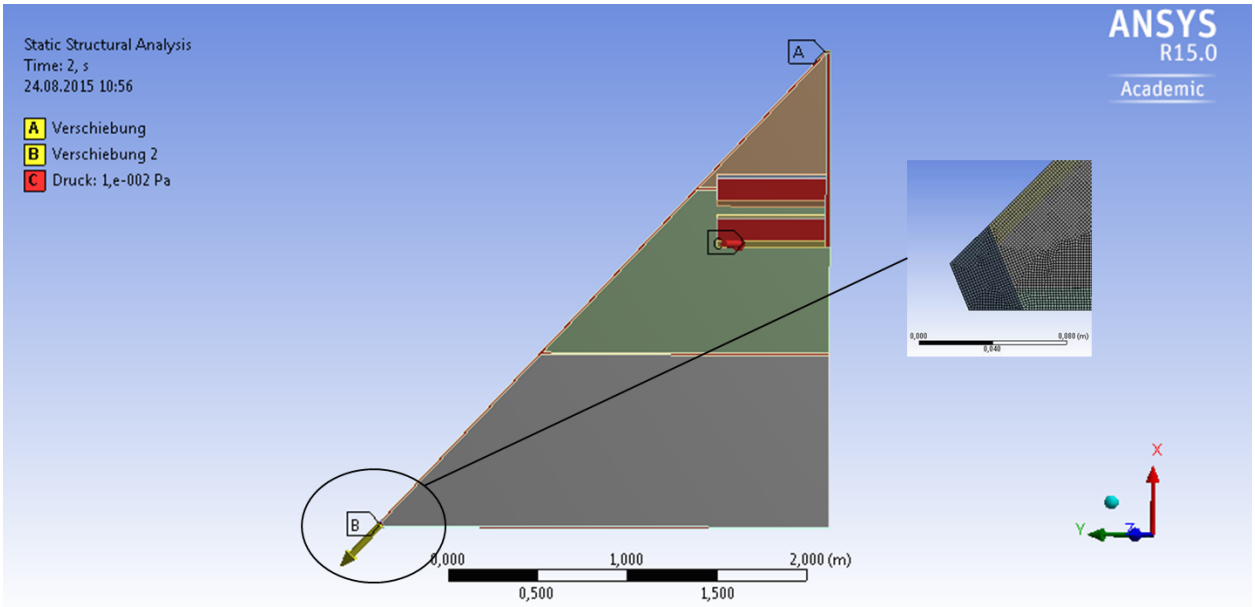

Figure 3. Geometry transferred into a finite-element shell model in ANSYS 15. Meshed homogeneously with quadratic shell-elements of edge length 1.5 $\times 10^{-3}$ m. At the inner edge, the displacement is set to zero. At the outer edge the displacement in negative x- and positive y-direction is set to 1.3 $\times$ 10^{-5} m. Pressure is applied along the z-direction on all surfaces.

membrane in a static case has to result in an equilibrium between internal and external forces. In addition, the wrinkles will appear so that an energy minimum of strain energy is achieved. Those effects can only be taken into account with a non-linear analysis as we have clearly at least a geometric non-linear process. In the analysis at hand, it was decided to use an implicit simulation. If the model converges in an equilibrium state, it is likely representing the real physical processes. The alternative would have been an analysis with explicit integration of the structural differential equations over time. This kind of simulation needs to be treated with much more care regarding its interpretation.

In order to resolve the wrinkling pattern in such a membrane, a very fine mesh is required so that a "wave" of one wrinkle is at least represented with four elements. If the mesh can not represent the wrinkling, it leads to a non-converging model. This means, the algorithm can not find the equilibrium between internal and external forces as this is generated by the wrinkling. The stronger the tension in the membrane the finer the wrinkling gets and in consequence one needs a finer mesh for the model to converge. For the loading considered here, elements with an edge length of 1.5×10^{-3} m were required.

The analysis is run in two steps. First the membrane is pretensioned in plane and in a second step the pressure is applied. When the membrane is pretensioned no wrinkling occurs because the membrane perfectly lies in one plane and thus can be loaded with compression loads. If then a small distortion is applied, in this case due to the pressure, the wrinkling occurs. This is comparable to a non-linear structural buckling analysis. The Gossamer-1 sail is only slightly tensioned. It is intended to have a

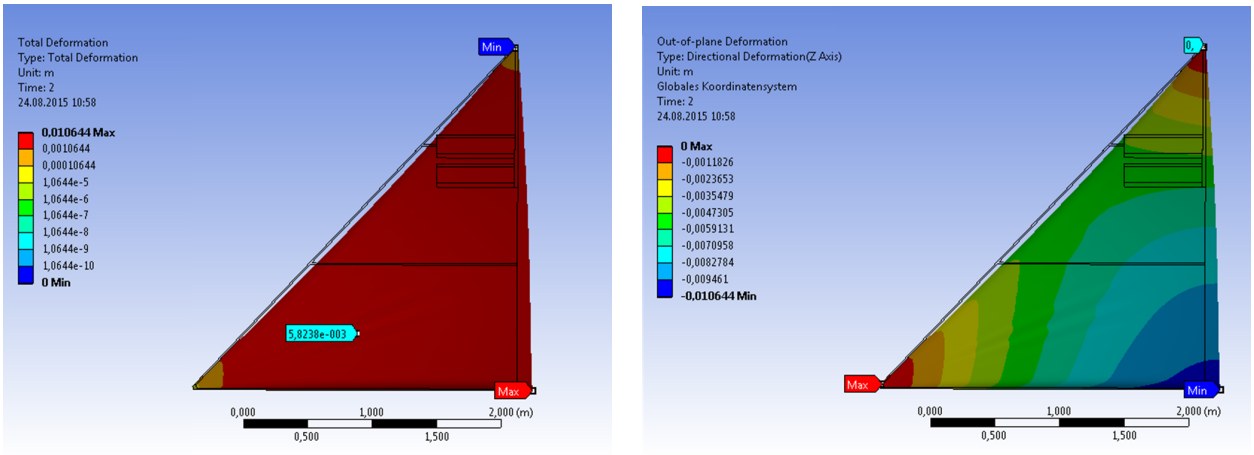

(a) Total Deformation (b) Out-of-plane Deformation

Figure 4. Resulting Deformation according to finite-element analysis

load of approximately 2 N. The load is applied by a displacement at the outer corner of 1.3×10^{-5} m in both x- and y- direction along the cathetus of the sail triangle (note that only the half triangle is shown in the pictures). The pretension is done in one load step. The simulation was intended to cover a pressure up to 10^{-2} Pa in order to take the orbit drag loads into account. The load was applied in 23 sub-steps and overall 56 iterations were required by the algorithm to find a converged solution.

The material data considered is given in Table 1. Note that except for the photovoltaic and harness area the Young's modulus of the Polyimide was considered in this approach and the Poisson's ratio was set to 0.3. In a future analysis, the material data may be considered in greater detail. All used materials are Polyimide foil with very thin coating. Therefore, the change of the values of the Young's modulus is very limited and will probably only have a minor impact on the overall results.

Table 1. Material Parameters, estimated by employing the Young's modulus of Upilex-S

Sail Area	Thickness [m]	Young's modulus [Pa]
Polyimide Foil	7.7×10^{-6}	9.69×10^{10}
Reinforcement, Bonding	4.97×10^{-5}	9.69×10^{10}
Thin-film Photovoltaic	1.14×10^{-4}	9.69×10^{10}
Photovoltaic and Harness	1.58×10^{-4}	1.85×10^{10}
Mid-Harness	6.9×10^{-5}	9.69×10^{10}

In order to further analyze the attitude behavior, the maximum out-of-plain displacement is described with a fitting function based on the results of the finite-element analysis. A function of the following type was chosen:

$$\Delta z = C \cdot \sqrt{p} \tag{1}$$

Here, Δz is the out-of-plane displacement, p is the pressure and $C = -0.11$ is the constant adjusted to the analysis results. The fitting has been obtained through a statistical linear regression of the type

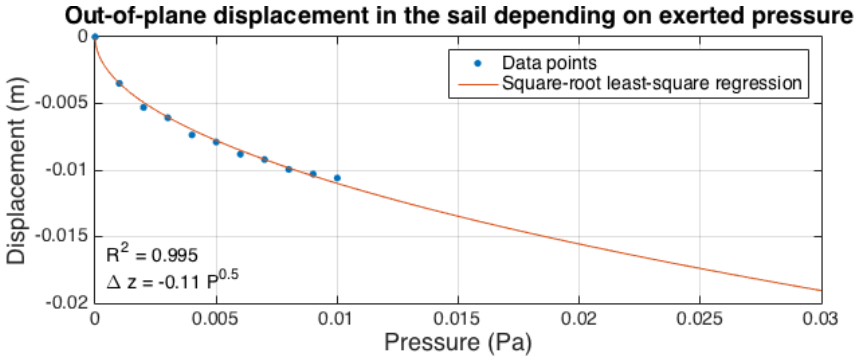

Figure 5. Maximum out-of-plane deformation of the sail membrane.

$y = \beta_0 + \beta_1 x$ and is shown in Figure 5. It is to be noted that the function is linear to the parameters β_i, while the variable x may be no linearly connected to y, as in this case.

After some statistical tests, the nullity of the parameter β_0 has been proved, in accordance with the physical model: in absence of pressure the sail is flat. It has to be underlined that, during the dynamics simulations, the maximum pressure reached is $P = 3 \cdot 10^{-2}$ Pa. This means that some values of the displacement will be extrapolated, because such values could not be simulated in the finite elements model.

3. Sail description

In Fig. 1(d) the structure of the deployed sail in Gossamer-1 is shown. Although presented as a flat sail, Section 2. shows that deformations take place in the out-of-plane direction when the sail is exposed to the drag force. Thanks to this structural investigation, it was possible to create a simplified model of the sail which could take into account its elasticity. To do so, the deformation visible in Fig. 4(b) has been analyzed and it has been decided to model the sail as a square, where the central edges of each quadrant can move along the out-of-plane direction, following the model fitted in Fig. 5 and shown in Eq. 1. This configuration can be seen in Fig. 6.

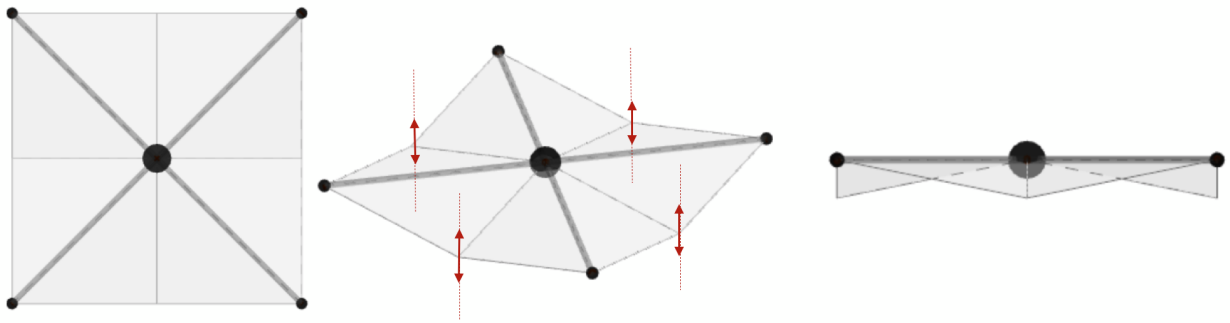

Figure 6. Simplified model of the sail used for dynamics simulations.

4. Dynamics model

In order to describe the orbit of a satellite and the motion of the satellite in its orbit, different reference frames were used. $(\mathscr{I}, (X_{\mathscr{I}}, Y_{\mathscr{I}}, Z_{\mathscr{I}}))$ is the Earth-fixed inertial reference frame, $(\mathscr{E}, (X_{\mathscr{E}}, Y_{\mathscr{E}}, Z_{\mathscr{E}}))$ is the Earth-Centered Earth-Fixed reference frame and $(\mathscr{B}, (X_{\mathscr{B}}, Y_{\mathscr{B}}, Z_{\mathscr{B}}))$ is the Body-fixed reference frame. The symbols for the reference frames are used in the paper as subscripts to indicate in which reference frame the variables are described.

To describe the angular velocity, attitude, position and velocity at least 12 variables are needed. In reality, to avoid singularities in the equations of motion, one redundant variable is added. Thus, the state vector consists of 13 variables in 13 equations: 7 variables for angular velocity and attitude in the form of quaternions $[\boldsymbol{\omega}, \overline{q}]$ to describe the rotational motion in the $\mathscr{B}$ reference frame and 6 variables for position and velocity $[\boldsymbol{r}, \boldsymbol{v}]$ to describe the translational motion in the $\mathscr{I}$ reference frame. The equations of motion are first-order Ordinary Differential Equations (ODEs) widely used in satellite dynamics: the Euler equation, the equation to update the quaternions and Newton's law in the form of two first-order ODEs. For both translational and rotational motion there are two vectorial equations, one describing the kinematics (how a change in attitude or position with time is characterized) and one kinetics (how a body responds to an applied torque or force).

$$\begin{cases} \dot{\boldsymbol{r}} = \boldsymbol{v} & \text{Translational motion, Kinematics} \\ \dot{\boldsymbol{v}} = -\dfrac{\mu}{r^3}\boldsymbol{r} + \boldsymbol{a} & \text{Translational motion, Kinetics} \\ \dot{\overline{q}} = \dfrac{1}{2}\overline{q} \otimes \overline{\boldsymbol{\omega}} & \text{Rotational motion, Kinematics} \\ \dot{\boldsymbol{\omega}} = I^{-1}\left(\boldsymbol{T} - \dot{I}\boldsymbol{\omega} - \boldsymbol{\omega} \times I\boldsymbol{\omega}\right) & \text{Rotational motion, Kinetics} \end{cases} \tag{2}$$

In the equations for the quaternion update, the angular velocity $\boldsymbol{\omega}$ has been transformed to the pure quaternion $\overline{\boldsymbol{\omega}} = [0\, \omega_x\, \omega_y\, \omega_z]^T$ to be able to exploit the quaternion product $\otimes$. The moment of inertia matrix I is not constant during the motion of the satellite due to the flexibility of the sail. For this reason the term containing $\dot{I}$ appears in the Euler equation. However, the term $\dot{I}\boldsymbol{\omega}$ is negligible due to the very small variations in the moment of inertia. Indeed the maximum deviation between the two matrices yields a relative error of 10^{-6}. Lastly, $\boldsymbol{a}$ and $\boldsymbol{T}$ are respectively a general perturbing acceleration and torque. Section 5. shows which perturbing forces and torques are influent on the sailcraft.

5. Perturbing forces and torques

The influent perturbations for a solar sail in low-Earth orbit, have been chosen after a first-order analysis. Figure 7 shows the variation of the perturbations with the altitude. It has to be underlined that the center of pressure(CoP)-center of mass(CoM) offset decreases with altitude, since it depends on the drag, hence this explains the different behavior between forces and torques. The plots show the perturbations down to 200 km: from this point the high forces may break the structure of the satellite, thus the mission is considered completed. The chosen perturbations are J_2, drag, solar radiation pressure and gravity gradient, as third-body perturbations are negligible for the range of altitudes considered.

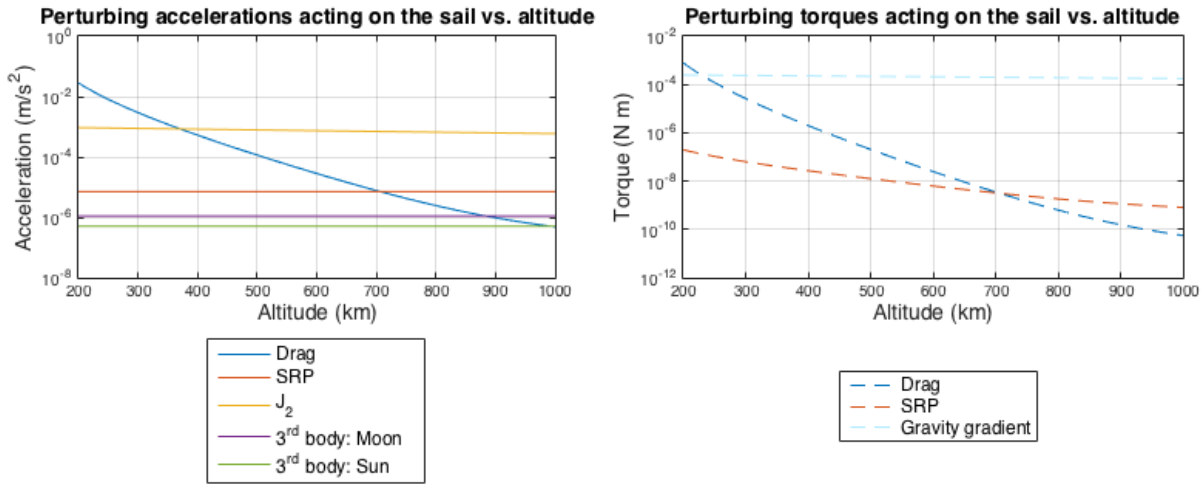

Figure 7. Perturbing accelerations and torques over altitude

The aerodynamic force is calculated in free molecular flow. Hypothesis and description of this model can be found in [12]. To calculate the density of the atmosphere, the NRL-MSISE-00 model has been assumed. The model considers mean solar cycle and variations of density during the day. Lastly, the aerodynamic coefficients can be calculated thanks to the model developed by Hart [13].

Solar radiation pressure has been implemented according to the non-ideal solar sail model by McInnes [14]: it takes into account absorption, diffuse reflection, specular reflection and transmission. Re-emission does not take place since both the back and front side of the sail are made of aluminum. When optical effects are taken into account, a non-negligible tangential component is created, while for ideal sails the force is directed only in the normal direction. To account for eclipses, a cylindrical model has been considered. Lastly, to determine the Sun position during the orbit in Earth-fixed inertial coordinates, an algorithm based on the Astronomical Almanac created by Vallado was chosen [15]. The algorithm approximates the ephemeris of the Sun with an accuracy of 0.01° for the Sun angular position.

To introduce the J_2 effect, the first term of the spherical harmonics for Earth's gravitational field is added in the acceleration vector. To do so, a transformation to the $\mathscr{E}$ reference frame is needed. The J_2 term well describes the main gravity perturbations with respect to the full model.

The gravity gradient torque is, for the most part of the de-orbit, the most influential torque on the satellite. This is due to the BSDUs at the tip of each boom which create a big moment of inertia. It is important to underline that, due to the symmetries in the sail ($I_x = I_y$), no torque is created along the $z_{\mathscr{B}}$ direction.

6. Integration

For the integration, several built-in Matlab integrators were analyzed. The most suitable method was found to be the Adams-Bashford-Moulton (ABM), a multistep method. Matlab implements a

variable-order ABM with the function `ode113`. To test the quality of the integrator both in results and speed, the integration of a Keplerian orbit was checked against the analytical solution. The tolerance of the integration has to be set by the user: the smaller the tolerance, the smaller the error between subsequent time steps, but the longer it takes for the simulation to give results. For this reason, a trade-off has been done and a relative and absolute tolerance of 10^{-7} was chosen, which results in a few centimeters loss for a one-month simulation.

7. Simplifications

Before starting the simulations, the hypotheses considered for the simulations are summarized:

- The model for a real solar sail is considered;
- The radiation Sun-satellite is linear;
- The density and temperature profile are modeled according to the NRL-MSISE-00 model;
- Eclipses are modeled with a cylindrical model;
- The drag determines the displacement in the sail;
- The displacement happens only in the $z_{\mathscr{B}}$ direction;
- The maximum rotation rate of the satellite before the deployment of the sail is $\omega_0 = 10°/\text{s}$.

8. Initial values

The initial position and attitude of the sail are only partially defined. For these reasons a grid search method was used to investigate the behavior of the sail. The only known parameter for the rotational behavior of the sail is the maximum rotation rate. It is estimated that the satellite will have an initial rotation rate ω_0 of $10°/\text{s}$ before deploying the sail. Approximating the deployment as an instantaneous event, the following equation holds: $I_0\boldsymbol{\omega}_0 = I\boldsymbol{\omega}$. After some algebraic manipulations, one reaches to the conclusion that the maximum rotation rate after deployment will be $\omega = 0.12°/s$.

Here the initial values for the simulation are shown:

- Position and velocity:
  The nominal orbit of the sail has a perigee altitude of 380 km, an apogee altitude of 700 km (corresponding to $a = Re + 540$ km and $e = 0.023$) and an inclination of $60°$. The other keplerian elements are not influent on the dynamics of the sail, thus they are just kept to zero. $\omega = 0°, \Omega = 0°, \theta = 0°$.
- Rotation rate:
  The sail may be still or moving, thus it has been chosen to simulate the following values: $\omega = [0, 0.012, 0.12]°/\text{s}$. Regarding the direction, the body axes with positive and negative direction are used, for a total of 6 possible directions. Since for $\omega = 0°/\text{s}$ no direction is required, the total number of combinations for the rotation rate is 13.
- Attitude:
  Even though it is not considered in the simulations, there is an initial state that possibly prevents the sail from re-entering. This happens when the angle of attack α is null and the sail is either still or rotates around $z_{\mathscr{B}}$. It is straightforward when an equatorial orbit is considered: indeed the satellite velocity and the relative velocity of the surrounding atmosphere are in the same plane and in the case where $z_{\mathscr{B}} = z_{\mathscr{J}}$ the drag area is zero, thus the drag perturbation does not affect the sail . This means that according to our model the sail stays flat and only the

gravity gradient torque and the forces due to SRP and J_2 affect its motion, without however affecting the angle of attack. In the simulations, initial conditions with different initial attitude around $z_{\mathscr{B}}$ are not considered due to the axial symmetries with respect to $x_{\mathscr{B}}$ and $y_{\mathscr{B}}$-axes. Also longitudinal rotations are in the interval $\lambda = [0, 180)^\circ$ while latitudinal rotation are in the interval $\phi = [0, 180)^\circ$ because of the symmetry of the sail. Choosing intervals of 45° for the sampling, the number of combinations for the attitude is 16.

This leads to 208 simulations.

9. Results

The first important question is to understand the influence that an elastic sail has on its motion. The CoM and the CoP are moved along the $z_{\mathscr{B}}$ axis during the motion thus creating torques due to drag and solar radiation pressure, which are not present in a flat sail, where CoP and CoM coincide. However, their influence is dependent on the initial pre-tensioning of the sail: the more the sail is tensioned to the booms, the less it billows, thus having a smaller CoP-CoM offset. Since the gravity-gradient torque is essentially constant with respect to pre-tensioning, as shown by the small difference in the moment of inertia matrix, it is interesting to compare the magnitude of the two torques.

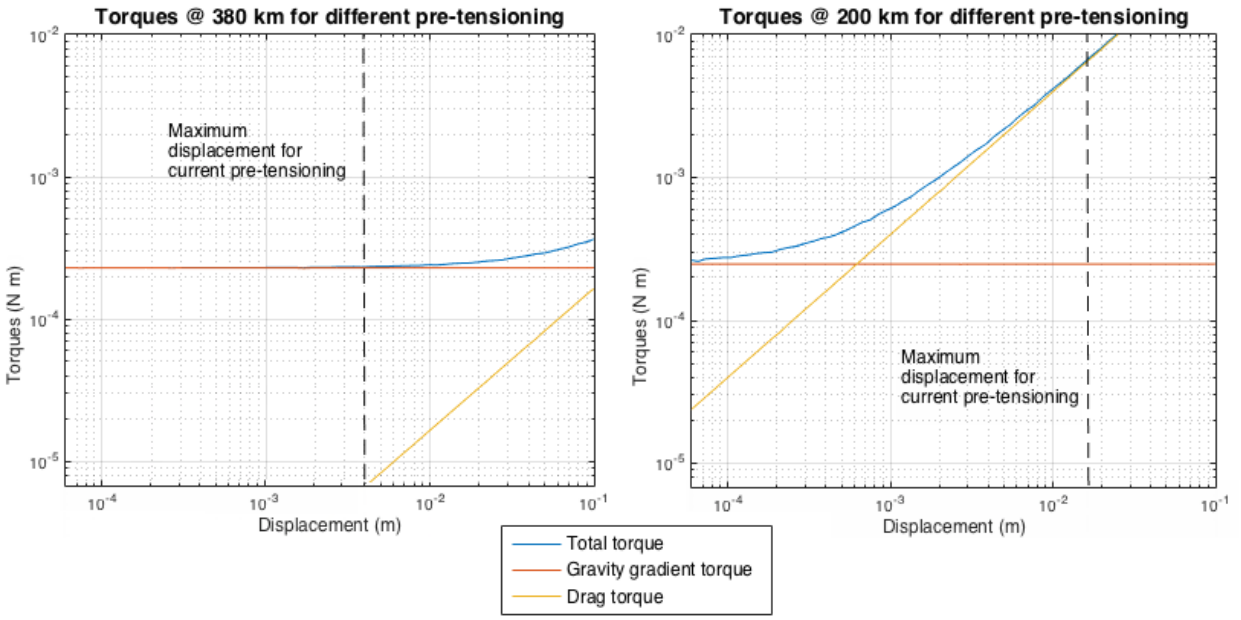

Figure 8. Maximum torque on the sail depending on maximum allowed billowing at 380 and 200 km.

Figure 8 shows the variation of torques depending on the maximum allowed billowing at 380 km, the initial perigee, and 200 km, the altitude at which the mission is considered completed. It can be seen that the drag torque is essentially linear with the displacement, since it is directly proportional to the CoP-CoM offset. It can be seen that for the current design, at 380 km the torque induced by the elasticity of the sail is small but not irrelevant, while towards the end-of-life it is the main

torque acting on the sail. These results support the initial hypothesis that the displacement in the sail cannot be neglected. To understand the influence of these torques, in Fig. 9 they are plotted for a de-orbit considering a flat sail and the elastic model.

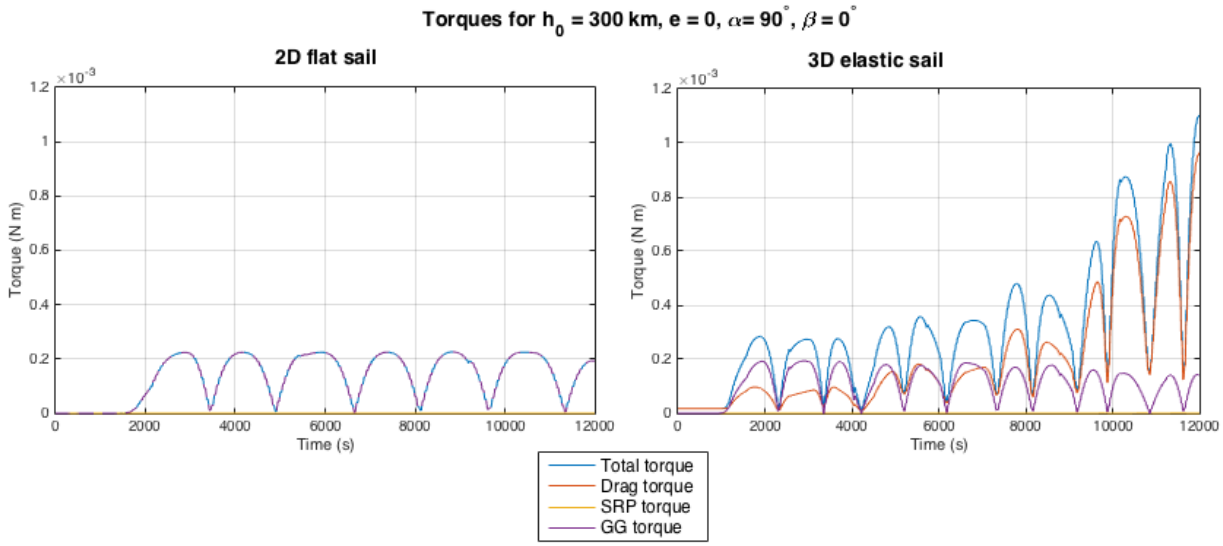

Figure 9. Torques acting on the sail for 2D and 3D model

From Fig. 9 one can notice that the magnitude of the gravity gradient is essentially unmodified when choosing a 2D or 3D sail, in accordance with the initial analysis on the moment of inertia matrix. The drag torque becomes the main torque during the de-orbit, underlined also in Fig. 8. For the same de-orbit one can also check that the initial forces acting on the sail are different, indeed the force applied on a flat sail is bigger: in the 3D model there are components developed in the $x_{\mathscr{B}}$ and $y_{\mathscr{B}}$ axes that are symmetrical and thus eliminated.

Regarding the de-orbit, the main concern was the possibility that the rotation rate would increase to critical values, thus resulting in the destruction of the sail before the de-orbit was completed. However, due to the big moment of inertia caused by the BSDUs, the satellite keeps rotating around the equilibrium points for the different torques, thus never abruptly increasing its rotation rate, reaching a maximum of 0.4°/s and always having a minimum close to or equal to zero, although the initial rotation rate is not null. This means that the sail is likely to complete the mission without problems due to high rotations.

For the sake of completeness, simulations were also done for a scenario with jettisoned BSDUs, foreseen for the future high-orbit launch of Gossamer-2, for the same initial orbit as Gossamer-1. The results show a smaller de-orbit time, but a much higher rotation rate. These results are in accordance with the theory: the same force applied on a lighter body yields a bigger acceleration, deceleration in this case; likewise a torque applied to a body with a smaller moment of inertia yields a bigger rotation rate.

Regarding the time of life, the simulations show a range of de-orbit times from 6 to 30 days,

as shown by Fig. 10.

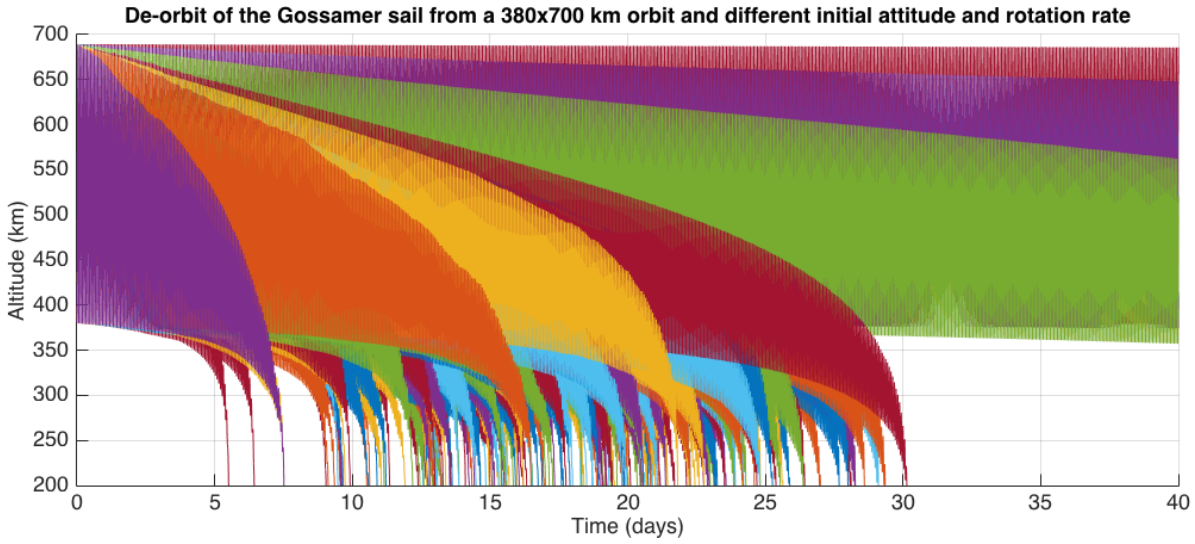

Figure 10. De-orbit times for different initial conditions on rotation rate and attitude

However, on initial configurations with small angle of attack, small side slip angle and rotation only around the $z_{\mathscr{B}}$, there is a range of values for which the de-orbit time significantly increases (visible in the non-deorbiting orbits if Fig. 10): the sail keeps oscillating around small values of the angle of attack, thus having only a small drag area, due to the gravity gradient action.

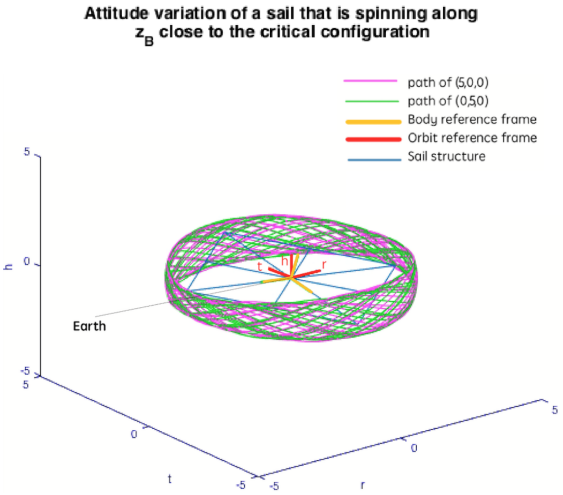

Figure 11. **Attitude variation of the sail for initial angle of attack $\alpha = 15°$, sideslip angle $\beta = 0°$ and rotation $\omega_z = 0.12°/s$. 10 days simulation.**

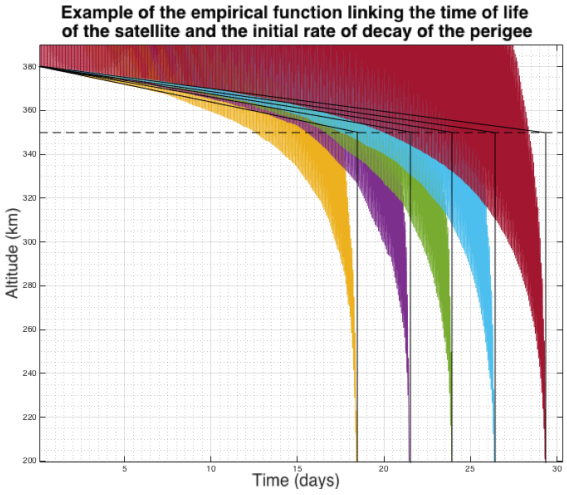

Figure 12. **Empirical function between time of life and initial rate of decay of perigee.**

This behavior is shown in Fig. 11. In case $\alpha = 0°$ the path created is just a circle around the $z_{\mathscr{B}}$ axis. The plot shows the in-orbit motion of the sail: the green and magenta lines show the path followed by the tips of the sail in $\mathscr{O}$. For these initial values a more dense grid search was performed

for varying values of the attitude and the magnitude of rotation rate, in order to understand how the time of life was affected. However, due to really high de-orbit times it was not possible to do the complete simulation, for this reason an alternative method was sought. Indeed, an empirical relation was found between the de-orbit time and the initial rate of decay of the perigee. Different simulations were considered and it was found that the intersection between the initial rate of decay of the perigee and the end-of-life time was always around the altitude of 350 km. Figure 12 shows the relation. Thanks to this relation, an estimate for the time of life could be retrieved with a linear transformation given the initial decay of the perigee for the orbits investigated around the critical values. Figure 13 shows contour plots with estimated time of life.

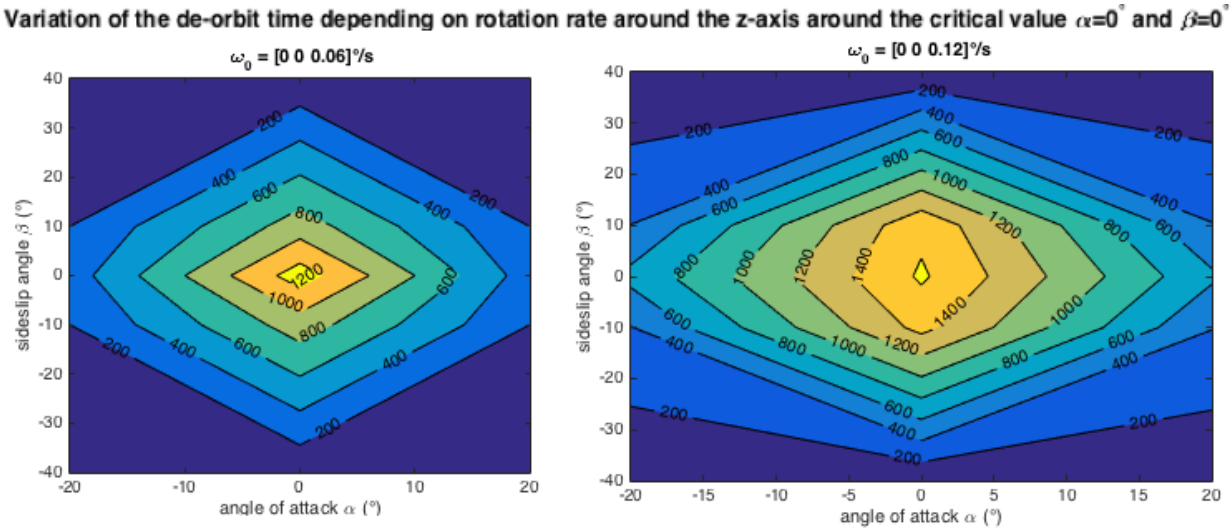

Figure 13. Variation of time of life (days) around critical value for different rotation rates.

This behavior was not detected for $\omega = 0°/s$ and $\omega_z = 0.012°/s$ in the initial search grid, which led to believe that the magnitude of the rotation rate played a role in this particular behavior. Indeed, from the contours it is clear that the behavior is enhanced for increasing values of the rotation rate. Being $\omega_{max} = 0.12°/s$, in the worst case scenario the sail would re-enter in 4 years. The same behavior was also detected for negative values of the rotation rate in a symmetrical manner. Furthermore, a sensitivity study was performed to understand whether perturbing rotations in the $x_{\mathscr{B}}$ and $y_{\mathscr{B}}$ axes would destabilize the motion or the pattern would be kept. The results showed that the faster the sail spins around the $z_{\mathscr{B}}$ axis, the lesser the same perturbation would affect the motion. However, rotations on other axes would significantly decrease the de-orbit time. For example, if $\omega_x = 10\%\,\omega_z$ and $\|\omega\| = 0.12°/s$, de-orbit is achieved in 500 days for $\alpha, \beta = 0°$, while for $\omega_x = 50\%\,\omega_z$ in 100 days and for $\omega_x = 90\%\,\omega_z$ in 23 days, which is a great difference from the 1400 days calculated for rotations only around $z_{\mathscr{B}}$. This behavior can be seen in Fig. 14. It has to be underlined that the pattern showed in Figure 11 is still present, due to the impossibility to dump the rotation in the $z_{\mathscr{B}}$ direction, but the ring shows increasing thickness for bigger perturbations, which means that the drag area increases and for this reason the de-orbit time is smaller.

Lastly, the situation where one sail fail to deploy was analyzed. In this case the sail would be asymmetric and thus some simulations were carried out to understand the behavior in such an

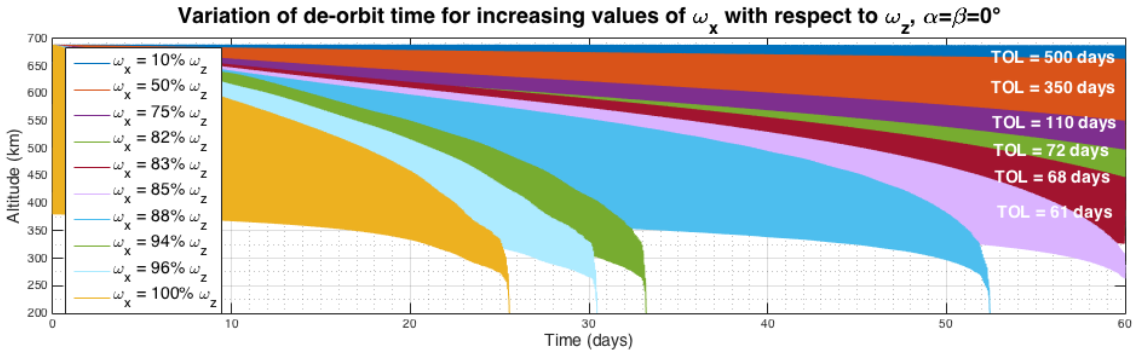

Figure 14. De-orbit times around critical values for increasing rotations around ω_x

unfortunate case. The results show higher rotation rates and torques developed also in the $z_{\mathscr{B}}$-axis as expected, however the maximum rotation rate reached is 2°/s which is still bearable by the structure. This means that in case one sail fails to deploy or breaks, the satellite can still re-enter without breaking apart in orbit.

10. Discussion and Conclusion

The analysis presented here shows the orbital and attitude dynamics of an elastic solar sail in low-Earth orbit. The main reason for modeling the elastic behavior was to understand if it had any effect on the behavior of the sail or a flat sail model would have given the same results. The simulations showed that for the conditions considered the torques developed due to the elastic behavior of the sail were not negligible. This conclusion is in accordance with the work by Sakamoto [16]. The main innovation was to complete a full dynamics model considering both the deformation of the sail due to forces in space and the effect that a deformed sail had on these forces.
The de-orbit simulations show that the sail reaches the altitude of 200 km in less than a month for the great part of initial conditions, apart from configurations close to zero angle of attack and initial rotation only in the $z_{\mathscr{B}}$ direction. These should be avoided if a fast de-orbit is wanted. However, if small perturbations in the other directions are present, the de-orbit time decreases significantly. More detailed results about the sensitivity of the de-orbit near critical values and output analysis can be found in [17].

11. References

[1] Wolff, N., Seefeldt, P., Bauer, W., et al. "Alternative Applications of Solar Sail Technology." M. Macdonald, editor, "Advances in Solar Sailing," Springer Praxis Book, 2014.

[2] Bonin, G., Hiemstra, J., Sears, T., and Zee, R. E. "The CanX-7 Drag Sail Demonstration Mission: Enabling Environmental Stewardship for Nano- and Microsatellites." "Proceedings of the 27th Annual AIAA/USU Conference on Small Satellites," 2013.

[3] Fernandez, J. M., Visagie, L., Schrenk, M., et al. "Design and development of a gossamer sail system for deorbiting in low earth orbit." Acta Astronautica, Vol. 103, pp. 204–225, 2014.

[4] Harkness, P. G. An aerostable drag-sail device for the deorbit and disposal of sub-tonne, low earth orbit spacecraft. Phd thesis, Cranfield University, 2006.

[5] Johnson, L., Whorton, M., Heaton, A., et al. "Nano Sail-D A solar sail demonstration mission." Acta Astronautica, Vol. 68, pp. 571–575, 2010.

[6] Lappas, V., Adeli, N., Visagie, L., et al. "CubeSail: A low cost CubeSat based solar sail demonstration mission." Advances in Space Research, Vol. 48, pp. 1890–1901, 2011.

[7] Pfisterer, M., Schillo, K., and Valle, C. "The Development of a Propellantless Space Debris Mitigation Drag Sail for LEO Orbits." "Proceedings of the WMSCI," 2011.

[8] Rankin, D., Kekez, D. D., Zee, R. E., et al. "The CanX-2 nanosatellite: Expanding the science abilities of nanosatellites." Acta Astronautica, Vol. 57, p. 167 174, 2005.

[9] Stohlman, O. R., Fernandez, M., Lappas, V. J., et al. "Testing of the Deorbitsail drag sail subsystem." "Proceedings of the 54 AIAA/ASME/ASCE/AHS/ASC Structures, Structural Dynamics, and Materials Conference," 2013.

[10] Seefeldt, P., Spietz, P., and Sproewitz, T. "The Preliminary Design of the GOSSAMER-1 Solar Sail Membrane and Manufacturing Strategies." "Advances in Solar Sailing," 2014.

[11] Seefeldt, P., Steindorf, L., and Sproewitz, T. "Solar sail membrane testing and design consideration." "Proceedings of the European Conference on Spacecraft Structures, Materials and Environmental Testing," 2014.

[12] Sentman, L. H. "Free molecule flow theory and its application to the determination of aerodynamic forces." Tech. rep., Lockheed Martin, 1961.

[13] Hart, K. A., Dutta, S., Simonis, K. R., Steinfeldt, B. A., and Braun, R. D. "Analytically-derived aerodynamic force and moment coefficients of resident space objects in free-molecular flow." "AIAA SciTech; 13-17 January 2014, National Harbor, Maryland," 2014.

[14] McInnes, C. R. Solar Sailing. Technology, dynamics and mission applications. Springer, 1999.

[15] Vallado, D. and McClain, W. Fundamentals of astrodynamics and applications. Managing Forest Ecosystems. Springer, 2001.

[16] Sakamoto, H., Park, K. C., and Miyazaki, Y. Effect of static and dynamic solar sail deformation on center of pressure and thrust forces. American Institute of Aeronautics and Astronautics, 2006.

[17] Pirovano, L. Attitude and orbital dynamics modeling for an elastic solar-sail in low-Earth orbit. Master's thesis, TU Delft, Work in Progress.